

Effect of excimer laser annealing on the silicon nanocrystals embedded in silicon-rich silicon nitride film

Rui Chen · D.F. Qi · Y.J. Ruan · S.W. Pan · S.Y. Chen ·
Sheng Xie · Cheng Li · H.K. Lai · H.D. Sun

Received: 21 April 2011 / Accepted: 26 August 2011 / Published online: 23 September 2011
© Springer-Verlag 2011

Abstract The investigations of silicon-rich silicon nitride film grown by plasma-enhanced chemical vapor deposition and then annealed by excimer laser have been carried out systematically. The surface roughness and the crystallization of the films have significantly been improved after the excimer laser annealing. The samples demonstrate visible photoluminescence emission under optical excitation at room temperature. It is found that the emission peak energy as well as emission intensity changes with laser annealing conditions, and the relevant mechanism is discussed in detail. Our investigation exhibits the size controllability of silicon nanocrystals embedded in the silicon nitride film, which implies promising applications in optoelectronic devices such as light-emitting diodes and solar cells.

1 Introduction

A lot of efforts have been devoted toward the silicon-based optoelectronic devices because of the low-cost manufactur-

ing and potential integration with matured silicon-based integrated circuits. Due to the indirect nature of its band gap, silicon demonstrates a very poor optical radiative efficiency. However, the light emission efficiency of silicon could be much enhanced when the size of silicon nanocrystals (nc-Si) is smaller than the free exciton Bohr radius of bulk silicon (~ 4.6 nm), which is well known as quantum confinement effect (QCE) [1–4]. In order to achieve the nc-Si, the silicon-rich silicon oxide (SRO) film has been generally introduced as the surrounding matrix [5]. In recent years, a great deal of research has been conducted and notable achievements have been witnessed by light-emitting devices (LED), solar cells, and thin-film transistors [6–11]. However, several problems remain to be resolved in this material system, such as the high operating voltage for carrier injection, and the localized levels due to the presence of silicon-oxygen double bonds [12]. Therefore, seeking appropriate matrix material for nc-Si is crucial for high efficiency room temperature photonic devices.

Silicon nitride, with a band gap of 5.3 eV, is considered as a better matrix material for nc-Si compared to silicon oxide [7]. The tunneling barrier of silicon nitride (1.5–2.0 eV) is lower than that of silicon oxide (3.1–3.8 eV), which enables easier carrier injection for electroluminescent devices [13]. Furthermore, replacing the oxide matrix by nitride also excludes the presence of silicon-oxygen double bonds, which helps to advance controllable tuning of the emission wavelength of nc-Si [14]. By introducing silicon nitride as matrix material, clear QCE and high emission efficiency have readily been achieved, and this also helps to clarify the light emission mechanisms underlying the nc-Si [15–17].

The technique to achieve different size of nc-Si is essential for some special applications such as full-color LED for display, and down conversion of high energetic photon for

R. Chen · D.F. Qi · Y.J. Ruan · S.W. Pan · S.Y. Chen (✉) · C. Li ·
H.K. Lai
Semiconductor Photonics Research Centre, Department of
Physics, Xiamen University, Xiamen, Fujian 361005, People's
Republic of China
e-mail: syichen@xmu.edu.cn

R. Chen · H.D. Sun (✉)
Division of Physics and Applied Physics, School of Physical and
Mathematical Sciences, Nanyang Technological University,
Singapore 637371, Singapore
e-mail: hdsun@ntu.edu.sg

S. Xie
School of Electronic Information Engineer, Tianjin University,
Tianjin 300072, People's Republic of China

solar cells. Generally speaking, several kinds of approach can be adopted to obtain different sizes of nc-Si in matrix materials, such as varying the ratio of the reactant gases and the temperature during the growth [18, 19]. In contrast, post thermal annealing is recognized as a simple and effective method to modify the property of the as-grown film. However, post annealing at temperatures as high as 1100°C is necessary for the formation and crystallization of nc-Si [20]. Such a high temperature is prohibitively high when integrating the device with other electronic components. Comparatively, excimer laser annealing (ELA) shows its unique advantages, including the easy control of the exposing area, and the low penetration depth under the ultraviolet wavelength [21, 22]. However, up till now, there is no systematic study on the ELA of silicon-rich silicon nitride (SRN) to provide a clear understanding on the annealing and emission mechanisms.

In this paper, silicon nitride is used as matrix material to embed nc-Si. We have systematically studied the influence of the ELA on the structure and optical properties of the SRN film. The evolutions of photoluminescence (PL) peak energy and emission intensity with different annealing conditions have been investigated and discussed in detail. Our result demonstrates the size controllability of nc-Si in SRN through simple ELA process, which provides useful information for future device application.

2 Experimental details

The SRN thin films used here were grown on a p-type silicon (100) wafer by plasma-enhanced chemical vapor deposition (PECVD), where nitrogen-diluted 10% SiH₄ and NH₃ with the purity of 99.9999% were used as the reactant gas sources. The flow rates of SiH₄ and NH₃ gas were fixed at 53 and 8 sccm, respectively. The plasma power, chamber pressure, and substrate temperature were maintained at 25 W, 2 Pa and 300°C during the growth, respectively. No in site annealing process was performed to form the nc-Si in SRN matrix after the growth. The thickness of the films was controlled ~100 nm.

The surface roughness of the SRN films before and after ELA was examined by means of atomic force microscopy (AFM). The local bonding configurations in the films were characterized by infrared absorption measurement on a Nicolet 380 Fourier transform infrared spectroscopy (FTIR) in the wave-number range from 400 to 4000 cm⁻¹. Raman analysis was performed on a Renishaw Raman spectrometer. The PL signal was dispersed by a 750 mm monochromator combined with suitable filters, and detected by a photomultiplier using the standard lock-in amplifier technique [23]. The response of detector and the efficiency of grating have been taken into account for reliable

PL intensity comparison [24, 25]. For both Raman and PL measurement, a He–Cd 325 nm laser was used as the excitation source.

3 Results and discussions

The as-grown SRN thin films were annealed by irradiating with 248 nm KrF excimer laser (from Lambda Physik), having a pulse width of 30 ns and a repetition rate of 10 Hz. Laser pulse densities ranging from 30 to 60 mJ/cm² were used. As schematically shown in Fig. 1(a), the film was placed in a quartz chamber which is transparent for the laser wavelength. During the annealing process, pure N₂ gas was introduced into the chamber and maintained at a constant flow rate to prevent oxidation. Subsequent surface analyses were performed by AFM, and typical three-dimensional (3D) profile images of the film before and after ELA are shown in Fig. 1(b) and 1(c). It can be seen that the as-grown film shows grains on the surface, while uniformity in size and smoothness of the surface are observed in the samples after ALE (30 mJ/cm² for 3 min). It is found that the surface roughness is improved from 1.22 to 0.95 nm. As mentioned before, the SRN films were grown at low temperature. The ELA process helps to achieve better crystallization of the film and thus better quality film can be obtained.

Figure 2(a) presents the transition FTIR spectrum of the as-grown SRN film, together with a pure silicon substrate for comparison. Apart from the Si–Si and Si–O bonds from the substrate, new peaks around 850 cm⁻¹ for Si–N stretching and 3360–3460 cm⁻¹ stretching modes for N–H bonds can be clearly observed [26], which confirms the successful growth of SRN film. As shown in Fig. 2(b), FTIR spectra of the SRN film under density of 45 mJ/cm² for different annealing time were recorded. Characteristic peaks ~1200 cm⁻¹ bending mode for N–H bonds, and 2100–2150 cm⁻¹ stretching vibration mode for Si–H bonds are

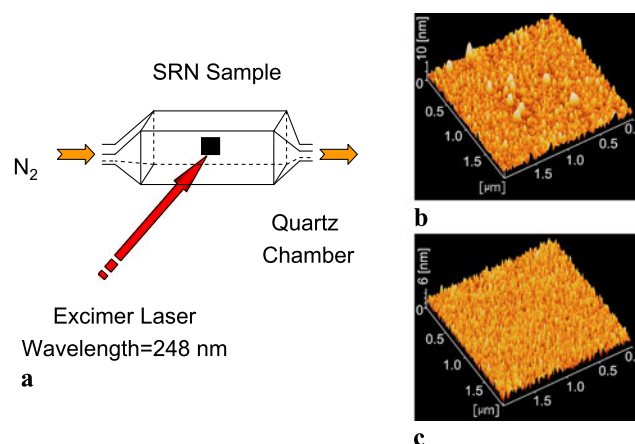


Fig. 1 (a) Schematic diagram of the ELA system. (b) and (c) is the AFM image of the SRN film before and after ELA

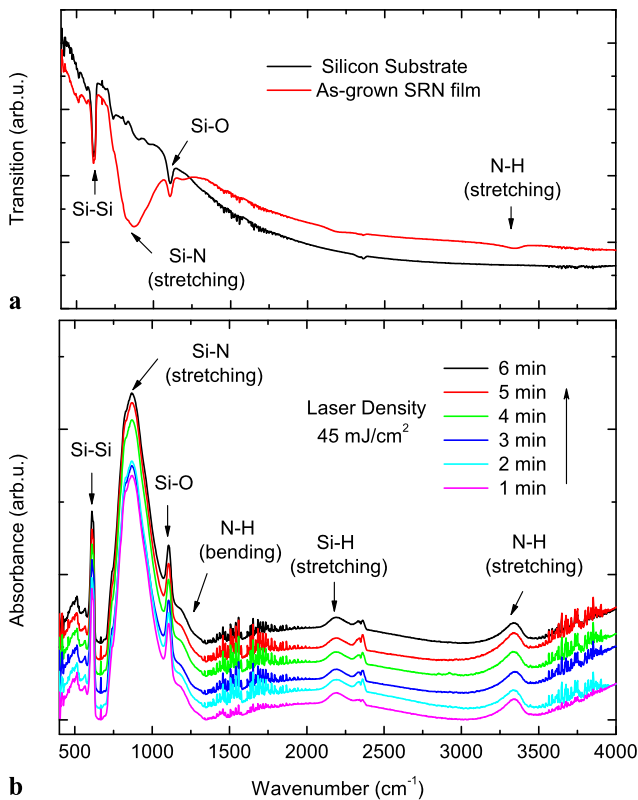


Fig. 2 (a) FTIR spectrum of the silicon substrate and SRN film. (b) FTIR spectrum of the SRN film after different annealing time

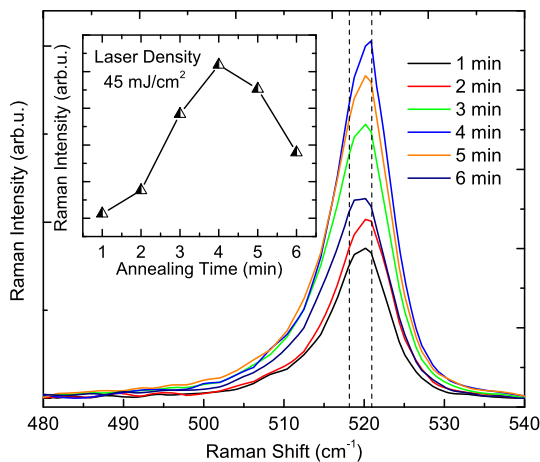


Fig. 3 Raman spectrum of the SRN film after different annealing time. Inset shows the intensity of the peak $\sim 518 \text{ cm}^{-1}$

easier to resolve in the absorption FTIR spectrum [26]. In fact, by changing the ELA time, not much difference between the FTIR data has been found. However, we need to mention that after annealing, hydrogen remains unchanged in the film. The resulting hydrogen produced from NH_3 is believed to not only improve the crystallization of nc-Si through hydrogen-induced crystallization, but also passivate the surface of nc-Si effectively [19, 27].

For the growth of the film, the ratio of the reactant sources (SiH_4 and NH_3) was controlled at 53:8, and thus the presence of nc-Si in the film after ELA can be expected. In order to confirm this, Raman measurement was carried out and the data were plotted in Fig. 3. As shown in the figure, the Raman spectrum exhibits a sharp and intense peak at 521 cm^{-1} due to silicon TO phonon mode from the substrate. At the low wave-number region, a shoulder can be found $\sim 518 \text{ cm}^{-1}$, the intensity of which changes with ELA time, and the corresponding relationship is drawn in the inset of Fig. 3. It is interesting to note that the Raman intensity increases with increasing ELA time from 1 to 4 min and then decreases for longer ELA time. The reason for this will be discussed later. Though the peak $\sim 518 \text{ cm}^{-1}$ is weak and only has a small shift compared with the peak at 521 cm^{-1} , it suggests the existence of nc-Si in the film after ELA. Based on the Richter (RWL) model [28], the analytical form was introduced to calculate the size of the nc-Si:

$$\Delta\omega = -\beta(a/D)^\gamma \quad (1)$$

where $\Delta\omega$ indicates the Raman frequency shift, a is the silicon lattice parameter ($a = 0.543 \text{ nm}$), and D is the cluster diameter, whereas the parameters β and γ for the model are 52.3 cm^{-1} and 1.586 , respectively. Based on the above equation, the size of the nc-Si is estimated to be $\sim 3.36 \text{ nm}$.

The observation strongly indicates the obvious improvement of crystallization of the film after ELA process, thus it should be very interesting to investigate the optical property of the samples. The normalized room temperature PL spectra (in linear scale) obtained from the samples under different ELA time are presented in Fig. 4. All the curves are shifted vertically for better clarity. For nc-Si embedded in matrix material, two different types of luminescent mechanism can be observed, namely, radiative recombination from defects in the film, and the emission of nc-Si due to QCE. Generally speaking, the PL peak position from the defect is believed to be less sensitive compared with QCE. As can be seen from Fig. 4, under different ELA time, the peak located at $\sim 2.75 \text{ eV}$ remains unchanged. It is revealed that this peak is related to the radiative recombination from silicon dangling bond ($\equiv \text{Si}^0$) to a twofold coordinated silicon centers (N-Si-O) [29, 30]. It is reasonable that small amount of oxygen will incorporate into the film to form the defect level, which has been confirmed by the FTIR measurement as shown in Fig. 2.

In contrast to this peak, another peak demonstrates a gradually red-shift with increasing ELA time. As predicted by the QCE, the band gap of the material will decrease when the size of a quantum structure increases. A red-shift in optical luminescence is the result of this effect. So the emission should be related to the carrier recombination from nc-Si in the SRN film. Assuming an infinite potential barrier, the

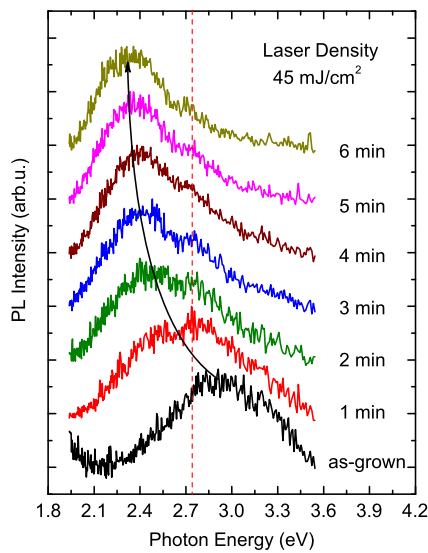


Fig. 4 Normalized PL emission from SRN film under different annealing time. Dashed line indicates the emission from defect level while solid line shows the change of photon energy with annealing time

energy gap of 3D confined of nc-Si in SRN film can be deduced from effective mass theory and expressed as [19]

$$E = E_{\text{bulk}} + C/D^2 \tag{2}$$

where $E_{\text{bulk}} = 1.13$ eV is the bulk crystal silicon band gap, $C = 13.9$ eV/nm² is the confinement parameter, and D is the size of nc-Si. From the experimental data, the size of the nc-Si is estimated to be ~ 2.76 nm for the as-grown SRN film and ~ 3.42 nm after ELA for 6 min. The values obtained verify the result from Raman measurement shown in Fig. 3. The reason why no shift of the Raman peak was observed may be the thin SRN film and the strong influence from the silicon substrate.

Figure 5 shows the comparison of the optical properties of the SRN films under various ELA laser densities and annealing times. As can be seen from Fig. 5(a), all the samples exhibit gradual red-shift of photon energy with increasing of ELA time. A closer look at the spectra reveals that smaller peak shift for laser density of 30 mJ/cm². It is understandable that for low laser density, the generated energy may not sufficient for creating bigger size of nc-Si compared to high laser densities. However, for laser density of 45 and 60 mJ/cm², no significant difference was observed, which indicates the excess of the threshold for crystallization. As shown in Fig. 5(b), all the samples demonstrate emission intensity increases with increasing ELA time from 1 to 4 min and then decreases at longer ELA time. This trend is in good consistence with the data shown in the inset of Fig. 3. It is known that successive laser annealing will continually introduce more defects (the incubation centers), which leads to a stronger absorbance. The increase in energy absorption

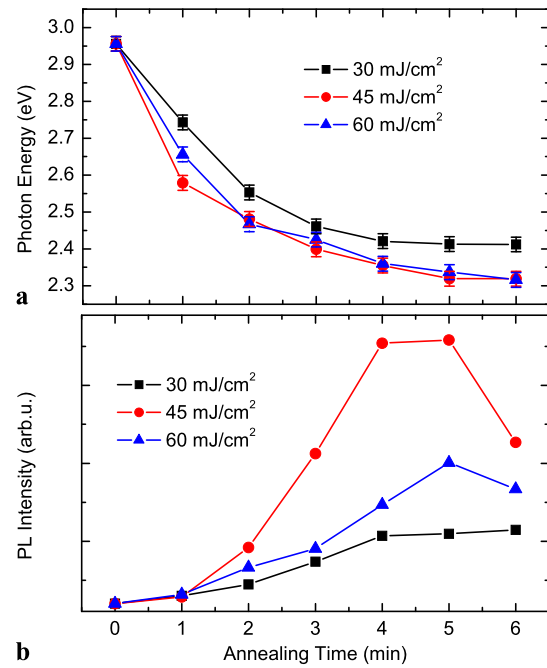


Fig. 5 The photon energy (a) and emission intensity (b) of the SRN film under different laser density as a function of annealing time

causes a decrease in threshold fluence, and laser ablation will start after certain annealing time [31]. From Fig. 5(b), it is also interesting to note that for a high laser density of 60 mJ/cm², the PL intensity always smaller than the samples annealing under laser density of 45 mJ/cm². Thus, it can be concluded that for ELA, the best annealing result can only be achieved at a certain time before laser ablation starts, and an appropriate laser density is also very important for ELA.

4 Conclusions

In summary, we have investigated the effect of ELA on the SRN film fabricated by PECVD at low temperature. It is demonstrated that the subsequent ELA induces obvious improvement of surface roughness and enables the formation of nc-Si in the film. The evolutions of Raman spectrum, PL photon energy, and emission intensity with the annealing condition have been investigated and discussed in detail. The results indicate that for ELA, proper laser density and annealing time should be carefully chosen to obtain desirable results. Our investigations exhibit the size controllability of nc-Si embedded in SRN film, which provides useful information for device application.

Acknowledgements Supports from the Nation Natural Science Foundation of China (NSFC) under grant Nos.: 50672079, 60837001 (Key Program), 61036002, National Basic Research Program of China (973 Program) under grant No. 2007CB613404, Natural Science Foundation of Fujian Province under grant No. 2008J0221, and the Singapore Ministry of Education through the Academic Research Fund (Tier 1) under Project No. RG63/10 are gratefully acknowledged.

References

1. T. van Buuren, L.N. Dinh, L.L. Chase, W.J. Siekhaus, L.J. Terminello, *Phys. Rev. Lett.* **80**, 3803 (1998)
2. N.M. Park, C.J. Choi, T.Y. Seong, S.J. Park, *Phys. Rev. Lett.* **86**, 1355 (2001)
3. B. Delley, E.F. Steigmeier, *Appl. Phys. Lett.* **67**, 2370 (1995)
4. E.F. Steigmeier, R. Morf, D. Grutzmacher, H. Auderset, B. Delley, R. Wessicken, *Appl. Phys. Lett.* **69**, 4165 (1996)
5. L.T. Canham, *Appl. Phys. Lett.* **57**, 1046 (1990)
6. C. Huh, K.H. Kim, B.K. Kim, W. Kim, H. Ko, C.J. Choi, G.Y. Sung, *Adv. Mater.* **22**, 5058 (2010)
7. N.M. Park, T.S. Kim, S.J. Park, *Appl. Phys. Lett.* **78**, 2575 (2001)
8. S.H. Choi, R.G. Elliman, *Appl. Phys. Lett.* **75**, 968 (1999)
9. Z.X. Ma, X.B. Liao, J. He, W.C. Cheng, G.Z. Yue, Y.Q. Wang, G.L. Kong, *J. Appl. Phys.* **83**, 7934 (1998)
10. Y.C. Chen, Y.S. Wu, I.C. Tung, C.W. Chao, M.S. Feng, H.C. Chen, *Appl. Phys. Lett.* **77**, 2521 (2000)
11. B. Zhou, S.W. Pan, R. Chen, S.Y. Chen, C. Li, H.K. Lai, J.Z. Yu, X.F. Zhu, *Solid State Commun.* **149**, 1897 (2009)
12. G. Allan, C. Delerue, M. Lannoo, *Appl. Phys. Lett.* **71**, 1189 (1997)
13. N.M. Park, S.H. Jeon, H.D. Yang, H. Hwang, S.J. Park, S.H. Choi, *Appl. Phys. Lett.* **83**, 1014 (2003)
14. M.V. Wolkin, J. Jorne, P.M. Fauchet, G. Allan, C. Delerue, *Phys. Rev. Lett.* **82**, 197 (1999)
15. Z.H. Cen, J. Xu, Y.S. Liu, W. Li, L. Xu, Z.Y. Ma, X.F. Huang, K.J. Chen, *Appl. Phys. Lett.* **89**, 163107 (2006)
16. Y. Wang, D. Shen, Y. Liu, J. Zhang, Z. Zhang, Y. Liu, Y. Lu, X. Fan, *Physica E* **27**, 284 (2005)
17. B.H. Kim, C.H. Cho, T.W. Kim, N.M. Park, G.Y. Sung, S.J. Park, *Appl. Phys. Lett.* **86**, 091908 (2005)
18. T.Y. Kim, N.M. Park, K.H. Kim, G.Y. Sung, Y.W. Ok, T.Y. Seong, C.J. Choi, *Appl. Phys. Lett.* **85**, 5355 (2004)
19. T.W. Kim, C.H. Cho, B.H. Kim, S.J. Park, *Appl. Phys. Lett.* **88**, 123102 (2006)
20. Y.Q. Wang, G.L. Kong, W.D. Chen, H.W. Diao, C.Y. Chen, S.B. Zhang, X.B. Liao, *Appl. Phys. Lett.* **81**, 4174 (2002)
21. C. Spinella, S. Lombardo, F. Priolo, *J. Appl. Phys.* **84**, 5383 (1998)
22. M. Hatano, S. Moon, M. Lee, K. Suzuki, C.P. Grigoropoulos, *J. Appl. Phys.* **87**, 36 (2000)
23. R. Chen, H.Y. Liu, H.D. Sun, *J. Appl. Phys.* **107**, 013513 (2010)
24. B. Liu, C.W. Cheng, R. Chen, Z.X. Shen, H.J. Fan, H.D. Sun, *J. Phys. Chem. C* **114**, 3407 (2010)
25. R. Chen, H.D. Sun, T. Wang, K.N. Hui, H.W. Choi, *Appl. Phys. Lett.* **96**, 241101 (2010)
26. D.V. Tsu, G. Lucovsky, M.J. Mantini, *Phys. Rev. B* **33**, 7069 (1986)
27. S. Sriraman, S. Agarwal, E.S. Aydil, D. Maroudas, *Nature* **418**, 62 (2002)
28. G. Faraci, S. Gibilisco, P. Russo, A.R. Pennisi, S. La Rosa, *Phys. Rev. B* **73**, 033307 (2006)
29. H. Nishikawa, T. Shiroshima, R. Nakamura, Y. Ohki, K. Nagasawa, Y. Hama, *Phys. Rev. B* **45**, 586 (1992)
30. D.P. Yu, Q.L. Hang, Y. Ding, H.Z. Zhang, Z.G. Bai, J.J. Wang, Y.H. Zou, W. Qian, G.C. Xiong, S.Q. Feng, *Appl. Phys. Lett.* **73**, 3076 (1998)
31. C.F. Tan, X.Y. Chen, Y.F. Lu, Y.H. Wu, B.J. Cho, J.N. Zeng, *J. Laser Appl.* **16**, 40 (2004)